# Growth of monodisperse nanospheres of $MnFe_2O_4$ with enhanced magnetic and optical properties*

M. Yasir Rafique[a)b)], Pan Li-Qing(潘礼庆)[a)†], Qurat-ul-ain Javed[b)], M. Zubair Iqbal[b)], Qiu Hong-Mei(邱红梅)[b)], M. Hassan Farooq[c)], Guo Zhen-Gang(郭振刚)[b)], and M. Tanveer[d)]

[a)] *College of Science and Research Institute for New Energy, China Three Gorges University, Yichang* 443002, *China*
[b)] *Department of Physics, University of Science and Technology of Beijing, Beijing* 100083, *China*
[c)] *School of Material Science and Engineering, University of Science and Technology of Beijing, Beijing* 100083, *China*
[d)] *Research Center of Materials Science, Beijing Institute of Technology, Beijing* 100081, *China*

(Received 6 February 2013; revised manuscript received 3 April 2013)

Highly dispersive nanospheres of $MnFe_2O_4$ are prepared by template free hydrothermal method. The nanospheres have 47.3-nm average diameter, narrow size distribution, and good crystallinity with average crystallite size about 22 nm. The reaction temperature strongly affects the morphology, and high temperature is found to be responsible for growth of uniform nanospheres. Raman spectroscopy reveals high purity of prepared nanospheres. High saturation magnetization (78.3 emu/g), low coercivity (45 Oe, 1 Oe = 79.5775 $A{\cdot}cm^{-1}$), low remanence (5.32 emu/g), and high anisotropy constant $2.84\times10^4$ $J/m^3$ (10 times larger than bulk) are observed at room temperatures. The nearly superparamagnetic behavior is due to comparable size of nanospheres with superparamagnetic critical diameter $D_{cr}^{spm}$. The high value of $K_{eff}$ may be due to coupling between the pinned moment in the amorphous shell and the magnetic moment in the core of the nanospheres. The nanospheres show prominent optical absorption in the visible region, and the indirect band gap is estimated to be 0.98 eV from the transmission spectrum. The prepared Mn ferrite has potential applications in biomedicine and photocatalysis.

**Keywords:** Mn ferrite, magnetic materials, hydrothermal method, superparamagnetic, Raman spectroscopy

**PACS:** 71.10.Ay, 75.50.–y, 75.75.–c, 78.67.Bf **DOI:** 10.1088/1674-1056/22/10/107101

## 1. Introduction

Nanostructures of magnetic transition oxides with spinel structure $MFe_2O_4$ ($M$ = Mn, Fe, Co, Ni, etc.) possess unique magnetic properties like moderate magnetizations, high coercivities, single domain effects, spin filterings, and so on,[1–3] which leads to impressive industrial and biological applications.[4,5] As an important member of the ferrite family, $MnFe_2O_4$ (MFO) has attracted noteworthy research interest due to its mesmerizing magnetic and electromagnetic properties. $MnFe_2O_4$ is partially inverse spinel so that the majority of $Mn^{2+}$ ions are located at tetrahedral (A) site while only 20% of them are located at octahedral (B) site.[6] The Mn ferrite ($MnFe_2O_4$) has a much lower resistivity than $CoFe_2O_4$ and $NiFe_2O_4$[7] and its magnetic moment is consistent with the Neel coupling scheme.[8] The bulk $MnFe_2O_4$ has a saturation magnetization of 80 emu/g, an anisotropy constant $K$ of $2.5\times10^3$ $J/m^3$, and exchange stiffness constant $A$ of $3.22\times10^{-12}$ J/m at room temperature (RT).[1,9,10] However, nanoparticles, nanostructures, and thin films of $MnFe_2O_4$ show diverse properties, such as, high anisotropy constant $K = 5.6\times10^4$ $J/m^3$,[10] size-dependent saturation magnetization (20 emu/g–70 emu/g),[11] and high Curie temperature.[12,13] Moreover, nanosized Mn ferrite (MFO) possesses super spin glass state,[14] superparamagnetism,[15,16] and RT spin filtering properties in epitaxial thin films.[17] These properties of MFO result in many attractive applications such as magnetic recording,[18] microwave, MRI contrast agent for liver imaging,[19] ferrofluid, water treatment,[20] site specific drug delivery,[21] magnetic tunnel junction-based sensor,[22] photocatalytic,[23] and water-splitting.[24]

To fabricate the nanoparticle of ferrites, a lot of research methods have been reported in the past a few years.[25] In the previous investigations, nanoparticles/nanostructures of $MnFe_2O_4$ have been synthesized by using various methods,[26] such as co-precipitation,[10] thermal decomposition,[27] microemulsions[28] and mechano-chemical[16] microwave-assisted[29] reverse micelles,[10,21] detonation of emulsion explosive,[30] polymerized complex method,[31] and solvothermal method.[32] Recently, nanorods,[33,34] nanospheres,[20,35] and a nano-octahedron[20] of $MnFe_2O_4$ have been synthesized by hydrothermal method. Guo *et al.*[23] reported on the synthesis of hollow spheres of 250-nm diameter by solvothermal method. Generally, ferrite nanoparticle/nanospheres grown by conventional chemical methods have low saturation magnetizations[11,16,21,27,32] due to dead layer effect and the presence of non-magnetic impuri-

*Project supported by the National Natural Science Foundation of China (Grant Nos. 50472092, 50672008, and 50971023), the Beijing Natural Science Foundation (Preparation and Magnetic Properties of Ferromagnetic Nanoring Lattice), and Research Foundation for Talented Scholars of China Three Gorges University. M. Y. Rafique was also supported by the Chancellor Scholarship of the University of Science and Technology of Beijing.

†Corresponding author. E-mail: lpan@ctgu.edu.cn

© 2013 Chinese Physical Society and IOP Publishing Ltd 

ties such as ferrihydrite. However, there is still the demand to synthesize uniform spherical nanoparticles of $MnFe_2O_4$ with high saturation magnetizations, low coercivities, and low remanent magnetizations for biomedical applications. Herein, we demonstrate a one-step, economical, surfactant-free, and efficient hydrothermal method of large-scale fabricating Mn ferrite nanospheres. The effect of reaction temperature on morphology is described. The nanospheres exhibit enhanced and unique magnetic properties. Furthermore, optical properties are also investigated for photocatalytic application.

## 2. Experimental details

### 2.1. Sample preparation

All chemicals were of analytical grade and directly used without purification. The 35-ml aqueous solution of 75-mM $MnCl_2{\cdot}4H_2O$, 150-mM $FeCl_2$, and 0.75-M NaOH was prepared in deionized water. In this protocol, the required weight of NaOH was dissolved separately in 10-ml deionized water and after the 10-min magnetic stirring of metal salt solution; it was added dropwise into metal salt. This suspension was further stirred to acquire the homogeneity for 10 min and 2-ml $N_2H_4{\bullet}H_2O$ was added as redox agent. Subsequently, the solution was transferred in a Teflon cup and sealed in a stainless steel autoclave. The temperature of the autoclave was maintained at 240 °C for 8 h, then it was cooled down to RT naturally. A dark brown product was collected at the bottom of the Teflon cup which was rinsed by water more than 5 times to remove the alkali salt and other impurities. The final product was obtained by drying in an oven at 45 °C for 10 h. The samples were also prepared at reaction temperatures of 140 °C, 180 °C, 200 °C, and 220 °C, keeping all the other conditions the same as those described above.

### 2.2. Characterization

The morphology and elemental composition of the prepared product was observed with field emission scanning electron microscope (FESEM) Zessis Ultra-5500. Rigaku smartlab X-ray diffractometer (XRD) was used for crystal structure and average crystallite size analysis. Tecnai F30 transmission electron microscope was used to characterize the microstructures. The scanning range was from 20° to 90° using Cu K$\alpha$ radiation ($\lambda$ value of 1.5406 Å). Raman spectrum was measured using Horiba Jobin Yvon HR 800 Raman spectrometer with excitation wavelength of 532 nm. Magnetic measurements were carried out using vibrating sample magnetometer (VSM) option of Quantum Design Versa Lab. Optical properties were investigated by measuring the transmission spectrum with Hitachi U-4100 spectrophotometer using solid sample measurement system.

## 3. Results and discussion

### 3.1. Structure, formation, and morphology

Figure 1(a) shows the X-ray diffractometer pattern of prepared Mn ferrite nanospheres. All diffraction peaks matched with the standard pattern of bulk Jacobsite MnFe2O4 (JCPDS 10-0319) and it confirms the cubic spinel structures. The average crystallite size calculated using Scherrer formula is 22 nm. No impurity and other phase related peaks are present in XRD pattern, which indicates the purity of the prepared sample. The lattice parameter calculated using refined d value and standard equation for cubic lattice is 8.48993 Å which is comparable to bulk value (8.499 Å) (JCPDS 10-0319). EDX spectrum (Fig. 2(b)) shows

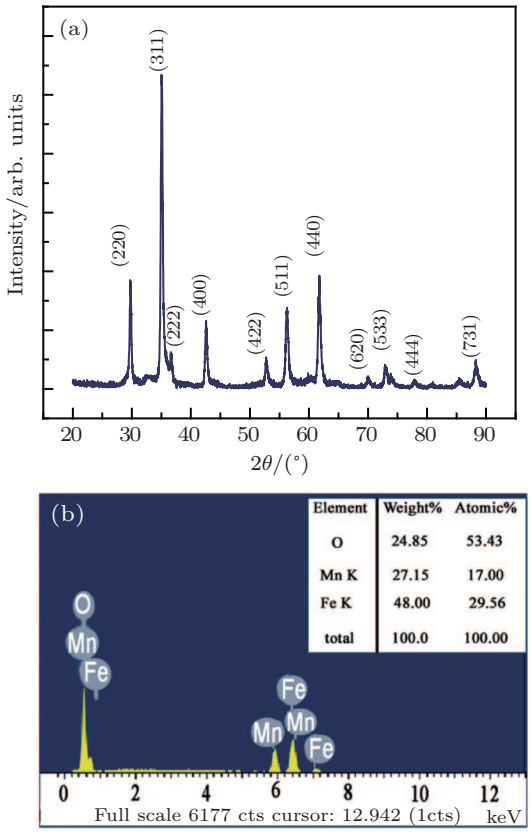



**Fig. 1.** (color online) (a) XRD pattern and (b) EDX spectrum of Mn ferrite nanospheres prepared at 240 °C.

only the peaks of Mn, Fe, and oxygen which further testify the purity of the sample. From the EDX analysis the elemental compositions for Mn, Fe, and oxygen are determined to be 17, 29.56, and 53.43 % respectively. The formation of $MnFe_2O_4$ nanospheres can be attributed to the chemical reaction as described by Eqs. (1)–(6). By addition of NaOH in the metal salts, the metal hydroxides were formed according to the following equation:

$$MnCl_2 \cdot 4H_2O + FeCl_2 + 4NaOH \rightarrow Mn(OH)_2 + Fe(OH)_2 + 4NaCl. \quad (1)$$

It is well known that hydrazine hydrate $N_2H_4$ can act as both oxidizing agent and reducing agent.[20] In our protocol, a com-

paratively small amount of hydrazine acts as oxidizing agent and oxidizes the $Fe(OH)_2$ into $Fe(OH)_3$ according to the following two equations:[20]

$$N_2H_4 + 2H_2O + 2e^- \rightarrow 2NH_3 + 2OH^-, \quad (2)$$

$$2Fe(OH)_2 + 2OH^- \rightarrow 2Fe(OH)_3 + 2e^-. \quad (3)$$

The metal hydroxide is not completely soluble in water and undergoes the reversible reaction as follows:

$$Fe(OH)_3 \leftrightarrow Fe^{3+} + 3OH^-, \quad (4)$$

$$Mn(OH)_2 \leftrightarrow Mn^{2+} + 2OH^-, \quad (5)$$

$$Mn^{2+} + Fe^{3+} + 8OH^- \rightarrow MnFe_2O_4 + 4H_2O. \quad (6)$$

Figure 2(a) shows an FESEM image of $MnFe_2O_4$ nanospheres at low magnification which shows high yield of nanospheres. Figure 2(b) shows an FESEM image at medium magnification of the prepared product which clearly indicates uniform nanospheres with diameters ranging from 45 nm to 60 nm. The shapes and uniformities of nanospheres are apparent from Fig. 2(c), indicating that the prepared nanospheres are nearly monodisperse. Moreover, neither agglomeration nor other structure of $MnFe_2O_4$ is observed from FESEM image. The size distribution of the nanospheres is calculated from Fig. 2(b) and it is shown in Fig. 2(d) which illustrates the narrow size distribution of the nanospheres, and the diameters of most of the nanospheres in a range of 45 nm–50 nm. The average diameter of the nanospheres is 47.3 nm with a standard deviation of 1.3 nm. The size distribution is fitted by Gaussian distribution with $R^2$ of value 0.975 and peak at 47.5 nm. The TEM image of the nanospheres is shown in Fig. 3(a), which shows the uniform nanospheres with an average size of about 50 nm, which is consistent with SEM images. The high resolution TEM (HRTEM) image of the nanospheres (Fig. 3(b)) shows that the boundary area of the nanosphere (shell) has an amorphous structure while the core is crystalline, indicating the core–shell structures of the nanospheres. The lattice fringes of the core indicate the single crystalline nature and from HRTEM image the lattice spacing is measured to be the 0.256 nm which corresponds to (311) lattice plane.

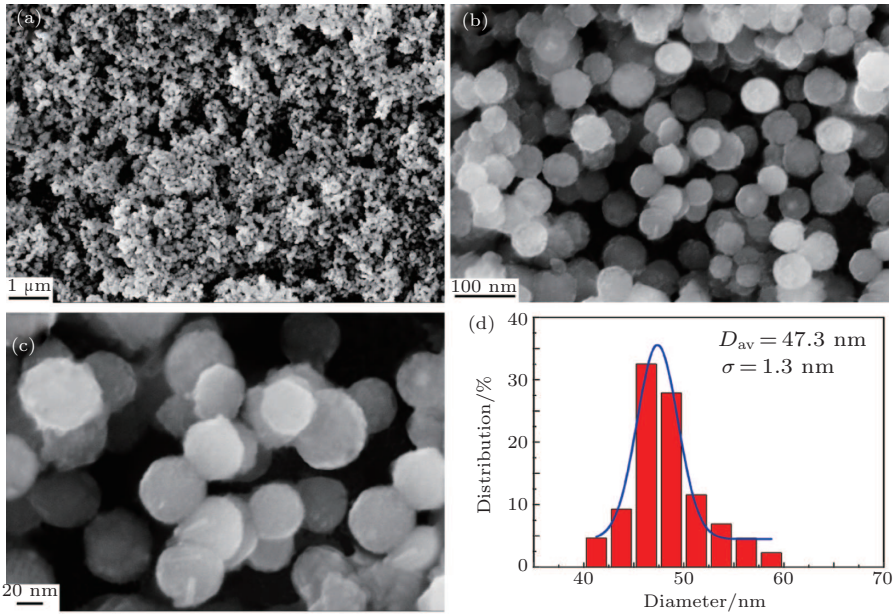



**Fig. 2.** (color online) FE-SEM images at (a) low, (b) medium, (c) high magnification, and (d) corresponding size distribution of $MnFe_2O_4$ nanospheres prepared at 240 °C.

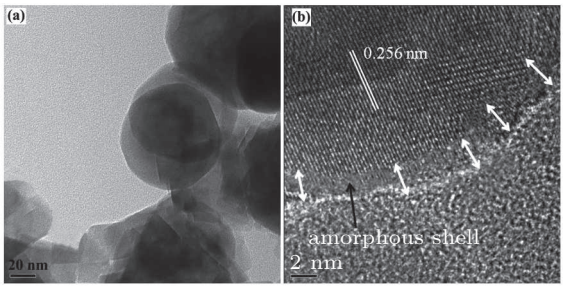



**Fig. 3.** (a) TEM image of nanosphere and (b) HRTEM image of nanosphere, the double headed arrows show the amorphous area.

### 3.2. Growth mechanism

In order to investigate the formation mechanism of $MnFe_2O_4$ nanospheres, a series of temperature-dependent experiments has been performed. Figure 4 shows FE-SEM images of samples prepared at different temperatures. The nanoparticles of sizes less than 30 nm were formed at a reaction temperature of 140 °C (Fig. 4(a)). By increasing the reaction temperature to 180 °C and 200 °C, larger particles of different shapes and sizes are grown as shown in Figs. 4(b) and 4(c) respectively. At a reaction temperature of 220 °C, most of

the particles present spherical shapes but having a wide distribution of sizes (Fig. 4(d). The nanospheres with a narrow size distribution are obtained by increasing the reaction temperature to 240 °C as shown in Fig. 2. From these results, it can be noted that the growth rate increases with reaction temperature increasing, as the size of particle increases with it. The high reaction temperature favors the growth of the spherical particle, because at a fast growth rate, the growth rates of various facets are the same, which results in isotropic morphology.[36] Furthermore, reaction temperature also facilitates the production of nanospheres with narrow size distribution.

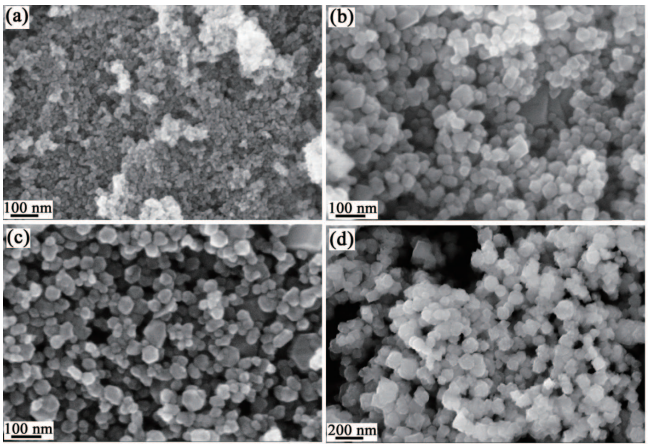



**Fig. 4.** FE-SEM images of samples prepared at reaction temperatures: (a) 140 °C, (b) 180 °C, (c) 200 °C, and (d) 220 °C.

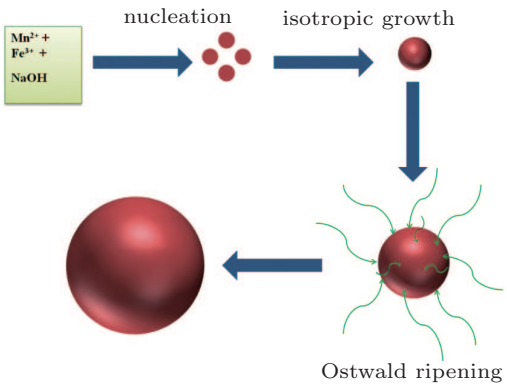



**Fig. 5.** (color online) Growth mechanism of nearly monodisperse nanospheres.

The possible growth mechanism of nanospheres is shown in Fig. 5. As the reaction takes place at a high temperature, the nucleation process occurs first by generating the small crystallites. These small crystallites start to grow along all directions under favorable thermodynamic conditions (isotropic growth). We suggest that Ostwald ripening starts immediately after nucleation which is responsible for uniform growth in all directions. Relatively fast nucleation process due to high concentration of metal ions ($Mn^{2+}$ and $Fe^{3+}$) and simultaneous nucleation of all species due to high reaction temperature result in narrow size distribution, whereas the fast growth process is responsible for spherical shape. Therefore nearly monodisperse nanospheres are generated.

### 3.3. Raman spectroscopy

Raman spectroscopy provides an important tool to probe the structural properties of synthesized materials.[37] It is sensitive to purity and many structural disorders such as lattice distortion, local cation distribution, structure transition, charge–lattice, and spin–lattice coupling, and magnetic ordering. For spinel ferrites ($MFe_2O_4$), it is a versatile tool for investigating the purity of the synthesized sample. The chemical synthesis of ferrite can introduce some nonmagnetic impurities such as 2-line ferrihydrite and 6-line ferrihydrite which cannot be detected by XRD pattern due to the overlapping of several peaks of ferrites with ferrihydrite phases.[38] However, the distinct peaks of ferrite and ferrihydrite in Raman spectra facilitate distinguishing them and determining their purities. $MnFe_2O_4$ has a cubic spinel structure that belongs to the space group $O_h^7$ ($Fd\bar{3}m$). The supercell contains 56 atoms, but the primitive cell only consists of 14 atoms ($Z = 2$). Therefore, 42 vibrational modes are possible. The factor group analysis predicts the five Raman active modes, i.e., $A_{1g} + E_g + 3T_{2g}$ in $MFe_2O_4$.[39] The Raman spectrum of prepared $MnFe_2O_4$ nanospheres in a frequency range of 200 $cm^{-1}$–1400 $cm^{-1}$ is shown in Fig. 6. The Raman spectrum consists of broad bands peaking respectively at 340, 456, and 563 $cm^{-1}$ and a strong band peaking at 646 $cm^{-1}$, which can be assigned to $E_g$, $T_{2g}(2)$, $T_{2g}(3)$, and $A_{1g}$ respectively. The mode $A_{1g}$ (646 $cm^{-1}$) is due to symmetric stretching of oxygen atoms at tetrahedral site. The other low frequency modes represent the characteristics of the octahedral sites ($BO_6$).[40] In the Raman spectrum, no impurity related modes are observed. The ferrihydrite phase has Raman-active modes at 710 $cm^{-1}$ and 1320 $cm^{-1}$,[38] which are clearly absent in the Raman spectrum of prepared nanospheres of $MnFe_2O_4$ (Fig. 6). Therefore, the Raman spectrum revealed the high purity of the prepared nanospheres.

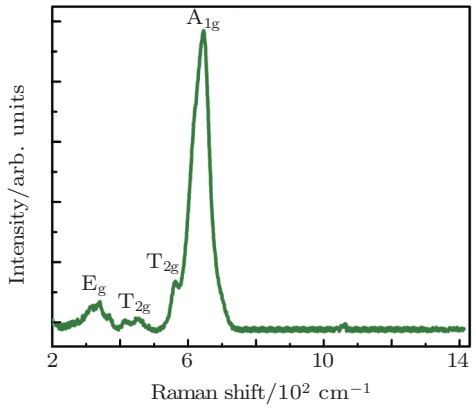



**Fig. 6.** (color online) Raman spectrum of Mn ferrite nanospheres measured in the ambient condition.

### 3.4. Magnetic properties

Magnetic hysteresis measured at RT is shown in Fig. 7(a). The saturation magnetization ($M_s$) of 78.3 emu/g is observed which is slightly less than the bulk value (80 emu/g).[1] Nevertheless, it is much greater than other reported values for nanoparticle, 200-nm and 1-μm nanospheres.[11,16,21,27,32] The high value of saturation magnetization (comparatively) is due to the absence of possible nonmagnetic impurities like ferrihydrite as evidenced from Raman spectrum. The coercivity of value 45 Oe is estimated at RT by linear fitting of data. The remanence is measured to be only 5.32 emu/g (squareness ratio $M_r/M_s = 0.067$) which is rather less than that of the assembly of three-dimensional (3D) noninteracting random particles with uniaxial anisotropy by Stoner–Wohlfarth (S–W) model ($M_r/M_s = 0.5$).[41] Low coercivity and low remanence point out that prepared nanospheres have nearly superparamagnetic behavior. The enlarged view of MH in the inset of Fig. 3(a) shows this nearly superparamagnetic behavior. The critical diameter $D_{cr}^{spm}$ for a spherical particle, below which the particle possesses the superparamagnetism, is given by the following formula:[3,42]

$$D_{cr}^{spm} = \left(\frac{6}{\pi}\frac{25k_BT}{K}\right)^{1/3}. \tag{7}$$

Using the value of $K$ for bulk material and $T = 300$ K, $D_{cr}^{spm}$ is calculated to be 42.9 nm, whereas the prepared nanospheres have an average diameter of 47.3 nm. Since the diameter of prepared nanospheres size is close to critical diameter $D_{cr}^{spm}$, nearly superparamagnetic behavior is observed. $M$–$H$ loop at $T = 60$ K is shown in Fig. 7(b) which indicates the saturation magnetization, coercivity, and remanence to be 91.3 emu/g, 280 Oe, and 22.86 emu/g, respectively (enlarged view in the inset of Fig. 7(b)). However, $M_s$ at $T = 60$ K is less than the bulk value (110 emu/g). The temperature dependence of magnetization of nanospheres is measured from 55 K to 400 K, shown in Fig. 7(c). $M$–$T$ curve indicates that blocking temperature is slightly above the 400 K (enlarged view in inset of Fig. 7).

The effective anisotropy coefficient can be calculated using a technical magnetization curve according to the law of approach to saturation given by Eq. (3),[43]

$$M(H) = M_s\left(1 - \frac{0.0762K_{eff}^2}{M_s^2H^2} - \cdots\right) + \chi_pH, \tag{8}$$

where $M(H)$, $K_{eff}$, and $\chi_p$ are magnetization at an applied field $H$, effective magnetic anisotropy constant $D_{cr}^{spm}$, and high field paramagnetic susceptibility respectively. By using the high field values from RT $M$–$H$ curve in Eq. (3), the effective anisotropy constant $K_{eff}$ is determined to be 2.84 J/m$^3$ which is 10 times higher than the bulk value,[9] which, however, is comparable to the value of the nanoparticle of Mn ferrite.[10] The prepared nanospheres have core–shell structure as evidenced from the HRTEM image (Fig. 3(a)). The core–shell structure of magnetic material has a well-ordered magnetic core surrounded by a shell having an amorphous magnetic structure. In the shell, poorly ordered magnetic moments could be isotropically pinned which can be coupled with magnetic moments of core and produce an effective magnetic drag on the core. Therefore, magnetic interaction between core and shell enhances the anisotropy of the nanospheres.[44,45]

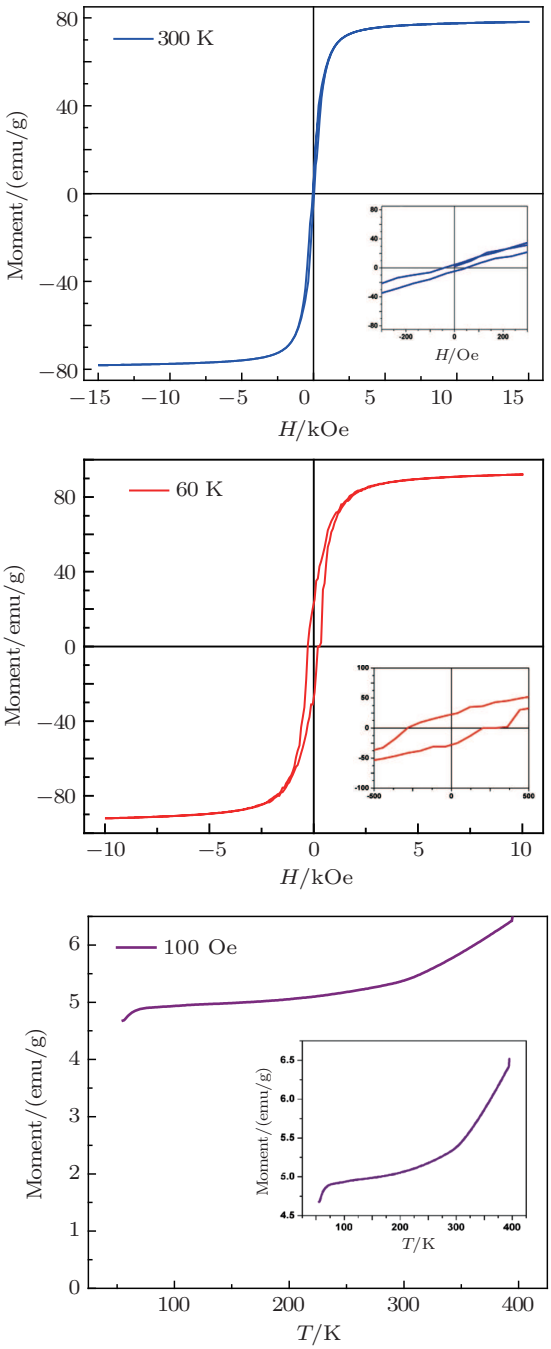



**Fig. 7.** (color online) Magnetic hysteresis loops of prepared nanospheres: (a) at $T = 300$ K and (b) at $T = 60$ K, and (c) temperature dependence of magnetization at $H = 100$ Oe (Insets show the enlarged views about origin).

### 3.5. Optical properties

To explore the potential application of $MnFe_2O_4$ as photo catalyst, its optical properties should be examined. In order to investigate the optical characteristic of $MnFe_2O_4$ nanospheres, the transmission/absorption spectra are recorded by UV-Vis spectrophotometer. Figure 8(a) shows the typical transmission spectrum of prepared Mn ferrite nanospheres with sizes in a range of 400 nm to 700 nm. It clearly shows the prominent absorption in the visible range. The optical band gap is an important parameter for optical characteristics and optical application. The optical band gap is related to absorption coefficient $\alpha$, which can be obtained from the transmission spectrum according the following equation:[46]

$$\alpha = \frac{1}{d}\ln\left[\frac{1}{T}\right], \tag{9}$$

where $d$ is the path length and in our case it is the width of cuvette, and $T$ is the transmittance. The optical band gap can be calculated by the following relation:

$$(\alpha h\nu)^2 = A(h\nu - e_g), \tag{10}$$

where $A$ is a constant, $E_g$ is the optical band gap, and $n$ is the exponent that depends on the nature of transition: $n = 2$ for direct band gap and $n = 1/2$ for indirect band gap. Therefore, the plots from Eq. (10) for the cases $n = 2$ and $1/2$ are shown in Figs. 8(b) and 8(c), respectively. It is clear from Figs. 8(b) and 8(c) that a straight line is obtained only for $n = 1/2$, indicating the indirect band gap nature. The value of the band gap is obtained to be 0.98 eV by extrapolating the linear fitted curve of $(\alpha h\nu)^{1/2}$ to energy axis at $\alpha = 0$. The narrow band gap value of 0.98 eV for $MnFe_2O_4$ is slightly larger than the calculated value for Mn ferrite.[47] Therefore, nanospheres of $MnFe_2O_4$ can have a photocatalytic application due to their strong absorptions in visible and narrow band gaps.

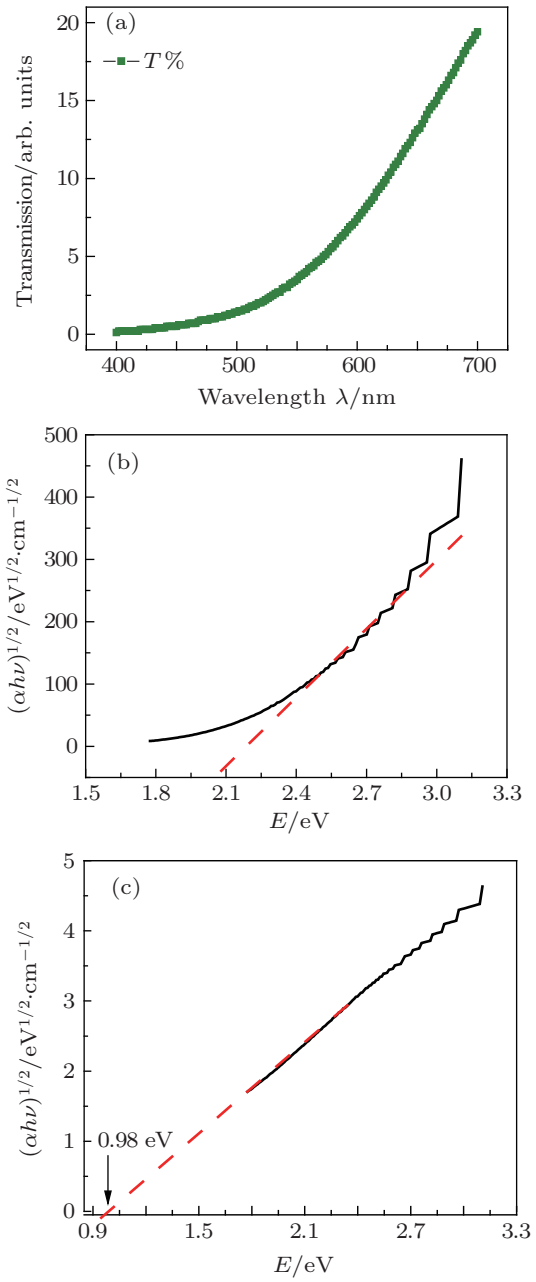



**Fig. 8.** (color online) Optical properties of $MnFe_2O_4$ nanospheres ; (a) transmission spectrum, (b) plot of $(\alpha h\nu)^2$ versus photon energy, and (c) plot of $(\alpha h\nu)^{1/2}$ versus photon energy (the dashed line represents the linear fitting).

## 4. Conclusions

Uniform nanospheres of $MnFe_2O_4$ are prepared by hydrothermal method without assistance of any surfactant. Diameters of nanospheres are in a range from 45 nm to 60 nm. The nanospheres have a narrow size distribution with an average size of 47.3 nm and a standard deviation of 1.3 nm. The reaction temperature affects the morphology remarkably, and the uniform nanospheres are grown at a high temperature of 240 °C. The characteristic Raman mode in Raman spectrum confirms Mn ferrite phase and high purity of sample. Nanospheres of $MnFe_2O_4$ have high saturation magnetization (78.3 emu/g), low coercivity (45 Oe), and low remanence (5.32) emu/g at 300 K. The nearly superparamagnetic behavior is due to the closer diameter of the prepared nanospheres to the critical diameter for superparamagnetism. Moreover, high effective anisotropy constant is due to core–shell structure. Nanospheres with such a narrow size distribution and magnetic properties have potential applications in biomedicine. Furthermore, nanospheres of Mn ferrite exhibit strong absorption in the visible region. The indirect band gap of value 0.98 eV is acquired from transmission spectrum. These optical characteristics of Mn ferrite nanospheres can have a photocatalytic application.

## References

[1] Bozorth R M, Tilden E F and Williams A J 1955 *Phys. Rev.* **99** 1788

[2] Masrour R, Hamedoun M and Benyoussef A 2012 *Chin. Phys. B* **21** 047501
[3] Rafique M Y, Pan L Q, Javed Q, Iqbal M Z and Yang L 2012 *J. Nanopart. Res.* **14** 1189
[4] Yu J, Huang D Y, Yousaf M Z, Hou Y L and Gao S 2013 *Chin. Phys. B* **22** 027506
[5] Li P, Jin C, Mi W B and Bai H L 2013 *Chin. Phys. B* **22** 047505
[6] Zuo X, Yang A, Yoon S, Christodoulides J A, Harris V G and Vittoria C J 2005 *J. Appl. Phys.* **97** 10
[7] Lotger F K 1964 *J. Phys. Chem. Solids* **25** 345
[8] Takadate K, Yamamoto Y, Makino A, Yamaguchi T and Sasada I 1998 *J. Appl. Phys.* **83** 6861
[9] Buschow K H J 1995 *Handbook of Magnetic Materials*, Vol. 8 (Amsterdam: Elesiver North-Holland) p. 212
[10] Adam J R, Chao L and Zhang Z J 2001 *J. Phys. Chem. B* **105** 7967
[11] Chen J P, Sorensen C M, Klabunde K J, Hadjipanayis G C, Devlin E and Kostikas A 1996 *Phys. Rev. B* **54** 9288
[12] Chinnasamy C N, Yang A, Yoon S D, Hsu K, Shultz M D and Carpenter E 2007 *J. Appl. Phys.* **101** 09
[13] Toshikam T 1999 *IEEE Trans. Magnet.* **35** 3010
[14] Aslibeiki B, Kameli P, Salamati H, Eshraghi M and Tahmasebi T 2010 *J. Magn. Magn. Mater.* **322** 2929
[15] Chao L and John Z 2001 *Chem. Mater.* **13** 2092
[16] Bellusci M, Aliotta C, Fiorani D, La Barbera A, Padella F, Peddis D, Pilloni M and Secci D 2012 *J. Nanopart. Res.* **14** 904
[17] Matzen S, Moussy J B, Mattana R, Bouzehouane K, Deranlot C and Petroff F 2011 *Phys. Rev. B* **83** 184402
[18] Sugimoto M 1999 *J. Am. Ceram. Soc.* **82** 269
[19] Lu J, Ma S L, Sun J Y, Xia C C, Liu C, Wang Z Y, Zhao X N, Gao F B, Gong Q Y, Song B, Shuai X T, Ai H and Gu Z W 2009 *Biomaterial.* **30** 2919
[20] Wang Y Q, Cheng R M, Wen Z and Zhao L J 2011 *Eur J. Inorg. Chem.* **42** 2942
[21] Liu C, Zou B S, Rondinone A J and Zhang Z J 2000 *J. Phys. Chem. B* **104** 1141
[22] Grancharov S G, Zeng H, Sun S, Wang S X, O'Brien S, Murray C B, Kirtley J R and Held G A 2005 *J. Phys. Chem. B* **109** 13030
[23] Guo P, Zhang G, Yu J, Li H and Zhao X S 2012 *Colloids, Surfaces A: Physicochem. Eng. Aspects.* **395** 168
[24] Seralessandri L, Bellusci M, Alvani C, La Barbera A, Padella F and Varsano F 2008 *J. Solid State Chem.* **181** 1992
[25] Shen L F, Wang T and Wang Y 2005 *Acta Phys. Sin.* **54** 3100 (in Chinese)
[26] Ahmed M A, Okasha N and El-Dek 2008 *Nanotechnology* **19** 065603
[27] Balaji G, Gajbhiye N S, Wilde G and Weissmuller J 2002 *J. Magn. Magn. Mater.* **242** 617
[28] Zheng J M, Wu X C, Zou B S and Wang Y J 1998 *J. Magn. Magn. Mater.* **183** 152
[29] Solano E, Perez-Mirabet L, Martinez-Julian F, Guzma'n R, Arbiol J, Puig T and Obradors X 2012 *J. Nanopart. Res.* **14** 1034
[30] Wang X H, Li X J, Yan H H, Xue L, Qu Y D and Sun G L 2008 *Appl. Phys. A* **90** 417
[31] Popa M, Bruna P, Crespo D and Morenoz J M C 2008 *J. Am. Ceram. Soc.* **91** 2488
[32] Yanez-Vilar S, Anchez-Andujar M S, Gomez-Aguirre C, Mira J, Senarıs-Rodrıguez M A and Castro-Garcıa S 2009 *J. Solid State Chem.* **182** 2685
[33] Zhen L, He K, Xu C Y and Shao W Z 2008 *J. Magn. Magn. Mater.* **320** 2672
[34] Wang J, Chen Q W, Hou B Y and Peng Z M 2004 *Eur. J. Inorg. Chem.* **2004** 1165
[35] Chen G, Wang J, Zhou L, Ma W, Zhang D, Ren F, Yan H, Qiu G and Liu X 2012 *J. Am. Ceram. Soc.* **95** 3569
[36] Xia Y, Xiong Y, Lim B and Skrabalak S E 2009 *Angew. Chem. Int. Ed.* **48** 60
[37] Guo X Y, Du Z L, Ding P, Liang E J, Zhang H R, Liu Y Z and Liu H 2003 *Acta Phys. Sin.* **52** 237 (in Chinese)
[38] Ayyappan S, Mahadevan S, Chandramohan P, Srinivasan M P, Philip J and Raj B 2010 *J. Phys. Chem. C* **114** 6334
[39] Gasparov L V, Tanner D B, Romero D B, Berger H, Margaritondo G and Forro L 2000 *Phys. Rev. B* **62** 7939
[40] Lazarevi Z Z, Jovaleki C, Recnik A, Ivanovski V N, Mitri M, Romcevi M J, Paunovi N, Ceki B D and Romcevi N Z 2011 *J. Alloys Compd.* **509** 9977
[41] Ibusuki T, Kojima S, Kitakami O and Shimada Y 2001 *IEEE Trans. Magnet.* **37** 2223
[42] Guimaraes A P 2009 *Principle of Nanomagnetism* (New York: Springer) p. 69
[43] Chikazumi S 1997 *Physics of Ferromagnetism* (New York: Oxford University Press) p. 506
[44] Kodama R H and Berkowitz A E 1999 *Phys. Rev. B* **59** 6321
[45] An J, Gong C D and Lin H Q 2001 *Chin. Phys. Lett.* **18** 419
[46] Ghosh P K, Ahmed S F, Jana S and Chattopadhyay K K 2007 *Opt. Mater.* **29** 1584
[47] Huang J R and Cheng C 2013 *J. Appl. Phys.* **113** 033912